A Bayesian geoadditive model for spatial disaggregation

Peer-reviewed author version

RUTTEN, Sara; NEYENS, Thomas; E CASTRO ROCHA DUARTE, Elisa & FAES, Christel (2026) A Bayesian geoadditive model for spatial disaggregation. In: Spatial statistics, 74 (Art N° 100979).

DOI: 10.1016/j.spasta.2026.100979
Handle: http://hdl.handle.net/1942/49005

A Bayesian Geoadditive Model for Spatial Disaggregation

Sara Rutten *[1], Thomas Neyens[1,2], Elisa Duarte[1], Christel Faes[1]

[1]Interuniversity Institute for Biostatistics and statistical Bioinformatics (I-BioStat), Data Science Institute (DSI), Hasselt University, Hasselt, Belgium
[2]L-BioStat, Department of Public Health and Primary Care, KU Leuven, Leuven, Belgium

Abstract

We present a novel Bayesian spatial disaggregation model for count data, providing fast and flexible inference at high resolution. First, it incorporates non-linear covariate effects using penalized splines, a flexible approach that is not typically included in existing spatial disaggregation methods. Additionally, it employs a spline-based low-rank kriging approximation for modeling spatial dependencies. The use of Laplace approximation provides computational advantages over traditional Markov Chain Monte Carlo (MCMC) approaches, facilitating scalability to large datasets. We explore two estimation strategies: one using the exact likelihood and another leveraging a spatially discrete approximation for enhanced computational efficiency. Simulation studies demonstrate that both methods perform well, with the approximate method offering significant computational gains. We illustrate the applicability of our model by disaggregating disease rates in the United Kingdom and Belgium, showcasing its potential for generating high-resolution risk maps. By combining flexibility in covariate modeling, computational efficiency and ease of implementation, our approach offers a practical and effective framework for spatial disaggregation.

Keywords: Laplace approximation, Geostatistics, Splines, Disease mapping

*Corresponding author. *E-mail address*: sara.rutten@uhasselt.be

1 Introduction

Developing high-resolution risk maps is an important task in many scientific disciplines, including epidemiology, ecology and environmental science. However, the response variable of interest is often only available as aggregated data over larger defined areas. Therefore, spatial disaggregation models recently became a popular area of research as these models aim to describe the variation of the variable of interest within aggregated areas, allowing for the construction of fine-scale maps (Pittiglio et al. 2018, Brus et al. 2018, Li et al. 2012, Keil et al. 2013). Recent research has expanded the goals and range of spatial disaggregation. For example Gramatica et al. (2021) introduced a Bayesian multiple-membership approach that links outcomes observed on different spatial supports by weighting spatial random effects. In another direction, Lee (2023) proposed a two-stage approach that disaggregates count data onto a fine spatial grid to identify risk boundaries in the resulting continuous surface. Hence, these studies highlight that disaggregation may serve different purposes, from reconciling data across mismatched areas to revealing fine-scale heterogeneity.

Diggle et al. (2013) introduced a Bayesian model to disaggregate spatial disease count data, based on an underlying log-Gaussian Cox process (LGCP). This approach can be used to combine data across multiple spatial scales, meaning that covariate data at a smaller spatial scale than the response data can be integrated. However, the method employs a data augmentation technique, resulting in high computation times. To deal with this issue, Johnson et al. (2019) introduced a spatially discrete approximation to the LGCP model (SDALGCP). Although this approach speeds up the estimation process significantly, the use of the Monte Carlo Markov chain (MCMC) algorithm still results in relatively high computation times. The SDALGCP model is implemented in the eponymous Rpackage `SDALGCP`.

Another approach is provided by a class of non-Bayesian spatial disaggregation methods

using the idea of composite link models (CLM), proposed by Thompson & Baker (1981). CLMs are extensions of generalized linear models, designed to link each observation to multiple predicted values. Assuming an underlying continuous spatial process that can be modeled as a high-resolution square lattice, the areal count can be viewed as the sum of the counts of the lattice cells within the area (Nandi et al. 2023). Hence, the structure of a composite link model can be retrieved. This idea has been applied for disaggregation purposes by Ayma et al. (2016), using the penalized composite link model approach (PCLM) of Eilers (2007) together with a mixed model strategy. This model has been extended to a spatial temporal context by Lee et al. (2022). Both models rely on a penalized spline evaluated over the spatial coordinates to capture the spatial process and therefore do not allow obtaining estimates of the underlying spatial correlation structure.

A solution to this problem comes in the form of the classical geostatistical kriging approach. Area-to-point (ATP) kriging has been introduced by Kyriakidis (2004). To solve the ATP kriging systems, a point-support semivariogram is needed. This function cannot be calculated directly from areal data but should be derived from a 'regularized' experimental semivariogram (Goovaerts 2006). Over the years, several methods have been proposed to address this difficulty (Pardo-Igúzquiza & Atkinson 2007, Goovaerts 2008, Nagle et al. 2011, Truong et al. 2014). The approach of Goovaerts (2008) has been implemented in an R-package called `atakrig` (Hu & Huang 2020). However, this method only serves the purpose of disaggregating, not allowing for the estimation of covariate effects. Although, this R-package is tailored to continuous data with a Gaussian assumption, Rcode to perform ATP Poisson kriging is available on GitHub (Payares 2024).

A Bayesian kriging approach that allows for the inclusion of covariates and avoids the pre-specification of a semivariogram, has been introduced by Nandi et al. (2023). Following the idea of a composite link model, their approach assumes that areal counts can be obtained by

summing the counts of all lattice cells within an area. In contrast to the models introduced by Ayma et al. (2016) and Lee et al. (2022), they include a spatial component that is assumed to follow a Gaussian process. For computational speed, Laplace approximation is used for model estimation. To deal with the potentially high computational burden arising from the inversion of the spatial covariance matrix, the `disaggregation` R package approximates Gaussian random fields (GRFs) using the Stochastic Partial Differential Equation (SPDE) framework (Lindgren et al. 2011). This requires the construction of a mesh, which can be technically challenging. In the special case of Gaussian data and a linear link function, Integrated Nested Laplace Approximation (INLA) (Rue et al. 2009), through the `R-INLA` package, can also be used to fit these models (Moraga et al. 2017), but it lacks flexibility in the case of other distributions. Unlike the composite link models, these kriging models provide an estimate of the underlying spatial correlation structure but they do not allow the flexible modeling of smooth covariates.

Another promising solution to the computational burden associated with the estimation of the Gaussian process used in kriging, comes from a low-rank approximation. Spline-based approaches have been proposed in geostatistical data analysis to flexibly model the spatial component, without the need for mesh construction. For example, Kammann & Wand (2003) introduced a geoadditive framework that combines a spline-based low-rank kriging approach with additive models that allow the inclusion of non-linear covariate relationships. It is important to note that, although a spline based approach is used, this low-rank approximation is linked to the underlying spatial correlation structure, allowing to obtain the relevant estimates. This geostatistical approach has been implemented in a Bayesian framework by Sumalinab et al. (2025). They use Laplace approximation to reduce computation time, compared to the traditional MCMC approaches. However, to the best of our knowledge, it has not been used for disaggregation purposes.

Despite the effectiveness of existing methods (Johnson et al. 2019, Ayma et al. 2016, Nandi et al. 2023), there remains a need for a spatial disaggregation technique that combines the estimation of the spatial correlation structure with flexible modeling of smooth covariate effects and is computationally fast. In this paper, we introduce a novel spatial disaggregation model for count data, using a spline-based low-rank kriging approximation and incorporating smooth covariate effects by the use of P-splines. Similar to the method of Nandi et al. (2023), this modeling approach can be linked to the idea of composite link models. By leveraging Laplace approximations, the proposed method efficiently estimates the posterior distribution of the regression coefficients, offering computational advantages compared to MCMC approaches (Gressani & Lambert 2018, Lambert & Gressani 2023, Sumalinab et al. 2025, Gressani et al. 2024).

In Section 2, we introduce the methodology behind the new spatial disaggregation method. In Section 3, a simulation study is conducted to investigate the performance of the model. Finally, in Section 4, the data needed to fit the model and the required user-defined implementation choices are outlined. Section 5 contains two applications of the method on a dataset containing mortality counts in Belgium and a dataset on primary biliary cirrhosis (PBC) incidence in Newcastle upon Tyne, UK.

2 Methodology

Consider a location $\boldsymbol{w}$ with coordinates $\boldsymbol{w} = (w_1, w_2)$. Assume the true (but latent) count at $\boldsymbol{w}$ is given by $y(\boldsymbol{w})$. Let $m(\boldsymbol{w})$ and $r(\boldsymbol{w})$ represent the population size (e.g., the population at risk) and intensity (e.g., the disease's incidence rate) at location $\boldsymbol{w}$, respectively. Then $y(\boldsymbol{w})$ can be modeled as a realization of a Poisson variable with mean $\mu(\boldsymbol{w}) = m(\boldsymbol{w})r(\boldsymbol{w})$, such that $E(y(\boldsymbol{w})) = \mu(\boldsymbol{w})$. Now, let Y_i represent the actual reported count in area R_i $(i = 1, \ldots, n)$. Diggle et al. (2013) argue that it is natural to treat these counts as

aggregated values, meaning that the average number of cases in area R_i can be expressed as:

$$\mu_i = \int_{R_i} m(\boldsymbol{w}) r(\boldsymbol{w}) d\boldsymbol{w}. \tag{1}$$

2.1 Continuous geoadditive model

A geostatistical model for the underlying intensity $r(\boldsymbol{w})$ can be formulated. Sumalinab et al. (2025) present a Bayesian P-splines based approach to geoadditive modeling, combining the flexibility of a generalized additive model with spatial smoothing. Their model can be formulated as follows:

$$\log(r(\boldsymbol{w})) = \beta_0 + \sum_{k=1}^{p} \beta_k x_k(\boldsymbol{w}) + \sum_{j=1}^{q} f_j(z_j(\boldsymbol{w})) + s(\boldsymbol{w}). \tag{2}$$

The covariates $x_1 \dots x_p$ are linear predictors whereas the covariates $z_1, \dots, z_q$ are included as non-linear functions. The non-linear functions are formulated as a P-spline:

$$f_j(z_j(\boldsymbol{w})) = \sum_{k=1}^{K} \theta_{jk} b_{jk}(z_j(\boldsymbol{w})), \quad j = 1, \dots, q,$$

in which $\boldsymbol{\theta}_j = (\theta_{j1}, \theta_{j2}, \dots, \theta_{jK})^T$ follows a Gaussian prior $(\boldsymbol{\theta}_j | \lambda_j) \sim \mathcal{N}_K(\mathbf{0}, (\lambda_j \boldsymbol{P})^{-1})$ with penalty parameter λ_j and matrix $\boldsymbol{P}$ derived from a difference matrix (Lang & Brezger 2004).

The spatial term $s(\boldsymbol{w})$ accounts for spatial correlation and is modeled through a classical kriging approach. To address the high computational cost of kriging, Sumalinab et al. (2025) employ a low-dimensional representation of the spatial component, building on the approach of Kammann & Wand (2003), who use the kriging covariance function as basis functions. Commonly used correlation functions are:

- Exponential: $R_\rho(\boldsymbol{d}) = \exp(-\rho\|\boldsymbol{d}\|)$,
- Matérn with $\nu = 3/2$: $R_\rho(\boldsymbol{d}) = \exp(-\rho\|\boldsymbol{d}\|)(1 + \rho\|\boldsymbol{d}\|)$,

- Spherical: $R_\rho(\boldsymbol{d}) = (1 - 1.5\rho\|\boldsymbol{d}\| + 0.5\rho^3\|\boldsymbol{d}\|^3)\mathbb{1}(\|\boldsymbol{d}\| \leq \rho^{-1})$,
- Circular: $R_\rho(\boldsymbol{d}) = (1 - \frac{2}{\pi}(\vartheta\sqrt{1-\vartheta^2} + \arcsin\vartheta))$ with $\vartheta = \min(\rho\|\boldsymbol{d}\|, 1)$,

where the parameter ρ represents the range parameter used in kriging and $\|\cdot\|$ refers to the Euclidean distance. Note that $\nu = 3/2$ for the Matérn function corresponds to the simplest Matérn function that results in differentiable surface estimates (Kammann & Wand 2003). The spatial component can then be modeled as,

$$s(\boldsymbol{w}) = \beta_{w1}w_1 + \beta_{w2}w_2 + \sum_{s=1}^{S}\phi_s(\rho)u_s + \epsilon(\boldsymbol{w}), \tag{3}$$

where $\phi_s(\rho) = R_\rho(\boldsymbol{w} - \boldsymbol{\kappa}_s)$ are the basis functions and the coefficients $\boldsymbol{u} = (u_1, \ldots u_S)^T$ are assumed to follow a multivariate normal distribution $(\boldsymbol{u}|\lambda_{spat}, \rho) \sim \mathcal{N}_S(0, (\lambda_{spat}\boldsymbol{\Omega_\rho})^{-1})$ where $\lambda_{\text{spat}} > 0$. The $S \times S$ matrix $\boldsymbol{\Omega_\rho} = R_\rho(\boldsymbol{\kappa}_s - \boldsymbol{\kappa}_{s'})$ is constructed using a subset of spatial coordinates $\boldsymbol{\kappa}_s$ $(s = 1, \ldots, S)$. Following Sumalinab et al. (2025), these knots can be chosen through the use of a space-filling algorithm (Johnson et al. 1990, Nychka & Saltzman 1998). The error term ϵ is included to account for inaccuracies arising from the low-rank approximation. These errors are assumed to follow a normal distribution with mean 0 and constant variance σ^2.

2.2 A spatial disaggregation model

Combining equation (1) and the geoadditive model in equation (2), we can assume that the reported counts Y_i are, conditional on $s(\boldsymbol{w})$, mutually independent Poisson variables with means:

$$\mu_i = \int_{R_i} m(\boldsymbol{w}) \exp\left(\beta_0 + \sum_{k=1}^{p}\beta_k x_k(\boldsymbol{w}) + \sum_{j=1}^{q} f_j(z_j(\boldsymbol{w})) + s(\boldsymbol{w})\right) d\boldsymbol{w}. \tag{4}$$

We can approximate integral (4) on a fine grid. Denote by $\boldsymbol{w_{il}}$ $(l = 1, \ldots, L_i)$ the L_i centers of the grid cells that intersect area R_i and let $a_i(\boldsymbol{w_{il}})$ represent the percentage of grid cell l, centered in $\boldsymbol{w_{il}}$, that is covered by R_i (Figure 1).

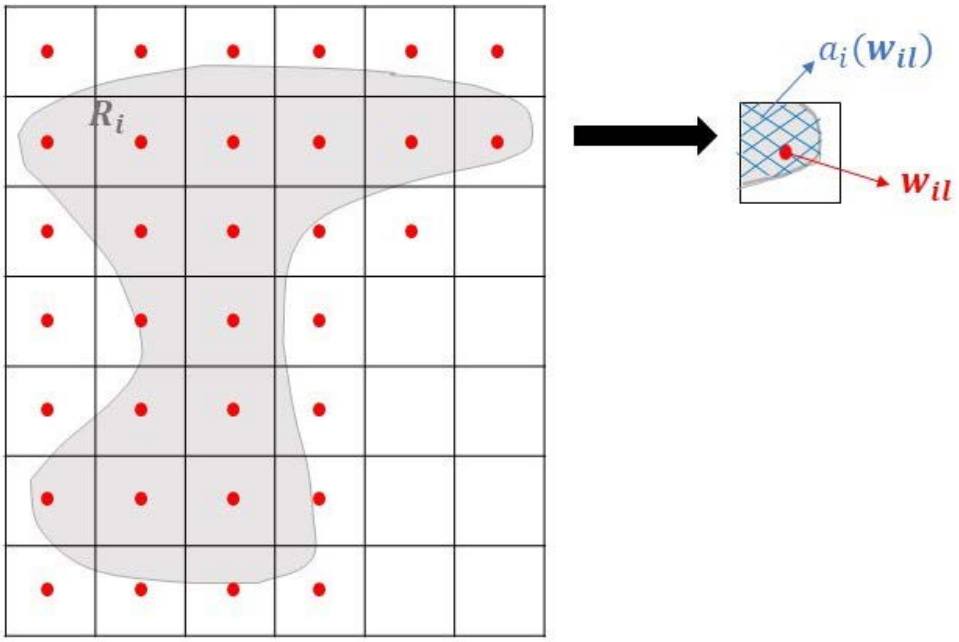

Figure 1: Visualization of the fine grid approach: in red, $\boldsymbol{w_{il}}$ $(l = 1, \ldots, L_i)$ denote the centers of the grid cells intersecting R_i and in blue, $a_i(\boldsymbol{w_{il}})$ denotes the percentage of a grid cell covered by R_i.

Then the approximation of integral (4) becomes:

$$\mu_i \approx \sum_{l=1}^{L_i} a_i(\boldsymbol{w_{il}}) m(\boldsymbol{w_{il}}) \exp\left(\beta_0 + \sum_{k=1}^{p} \beta_k x_k(\boldsymbol{w_{il}}) + \sum_{j=1}^{q} f_j(z_j(\boldsymbol{w_{il}})) + s(\boldsymbol{w_{il}})\right). \tag{5}$$

Following equation (3), we model the smooth term as:

$$s(\boldsymbol{w_{il}}) = \beta_{w1} w_{1il} + \beta_{w2} w_{2il} + \sum_{s=1}^{S} \phi_{ils}(\rho) u_s + \epsilon_i,$$

with $\phi_{ils}(\rho) = R_\rho(\boldsymbol{w_{il}} - \boldsymbol{\kappa}_s)$. Since the response data are available at the areal level, we include an area-specific independent random effect ϵ_i, representing a population-weighted average of the error terms at the fine grid, i.e.,

$$\epsilon_i = \frac{\sum_{l=1}^{L_i} a_i(\boldsymbol{w_{il}}) m(\boldsymbol{w_{il}}) \epsilon(\boldsymbol{w_{il}})}{\sum_{l=1}^{L_i} a_i(\boldsymbol{w_{il}}) m(\boldsymbol{w_{il}})}.$$

Therefore, they are modeled as $\epsilon_i \sim \mathcal{N}\left(0, \frac{\sum_{l=1}^{L_i} (a_i(\boldsymbol{w_{il}}) m_i(\boldsymbol{w_{il}}))^2}{\left(\sum_{l=1}^{L_i} a_i(\boldsymbol{w_{il}}) m_i(\boldsymbol{w_{il}})\right)^2} \sigma^2\right)$.

In matrix notation, the model can be formulated as:

$$\boldsymbol{\mu} = \boldsymbol{A_1} \exp(\boldsymbol{X\beta} + \sum_{j=1}^{q} \boldsymbol{B_j(z_j)\theta_j} + \boldsymbol{\Phi(\rho)u} + \boldsymbol{E\epsilon}),$$

where $\boldsymbol{\mu} = (\mu_1, \ldots, \mu_n)^T$. Let $N = \sum_{i=1}^{n} L_i$. Then X is a design matrix of dimension $N \times (p+3)$, where $\boldsymbol{X} = (\boldsymbol{X_1}^T, \ldots \boldsymbol{X_n}^T)^T$ with the l-th row of $L_i \times (p+3)$ dimensional matrix $\boldsymbol{X_i}$ given by $(1, x_1(\boldsymbol{w_{il}}), \ldots, x_p(\boldsymbol{w_{il}}), w_{1il}, w_{2il})$ and coefficient vector $\boldsymbol{\beta} = (\beta_0, \beta_1, \ldots, \beta_p, \beta_{w1}, \beta_{w2})^T$. Similarly, $\boldsymbol{B_j(z_j)}$ is an $N \times K$ matrix $\boldsymbol{B_j(z_j)} = (\boldsymbol{B_{j,1}(z_j)}^T, \ldots, \boldsymbol{B_{j,n}(z_j)}^T)^T$ and the l-th row of $L_i \times K$ dimensional matrix $\boldsymbol{B_{j,i}(z_j)}$ is equal to $\Big(b_{j1}(z_j(\boldsymbol{w_{il}})), \ldots, b_{jK}(z_j(\boldsymbol{w_{il}}))\Big)$. The coefficient vector $\boldsymbol{\theta_j} = (\theta_{j1}, \theta_{j2}, \ldots, \theta_{jK})^T$. Also, $\boldsymbol{\Phi(\rho)}$ is a $N \times S$ matrix with $\boldsymbol{\Phi(\rho)} = (\boldsymbol{\Phi_1(\rho)}^T, \ldots, \boldsymbol{\Phi_n(\rho)}^T)^T$ and the l-th row of $L_i \times S$ dimensional matrix $\boldsymbol{\Phi_i(\rho)}$ is equal to $(\phi_{il1}(\rho), \phi_{il2}(\rho), \ldots, \phi_{ilS}(\rho))$. The coefficient vector $\boldsymbol{u}$ is equal to $\boldsymbol{u} = (u_1, u_2, \ldots, u_S)^T$ and $\boldsymbol{\epsilon}$ is a n-dimensional vector $(\epsilon_1, \ldots \epsilon_n)^T$. Matrix $\boldsymbol{E}$ is a $N \times n$ design matrix with column i equal to

$$(\underbrace{0, \ldots, 0}_{\sum_{l=1}^{i-1} L_l \text{ times}}, \underbrace{1, \ldots, 1}_{L_i \text{ times}}, \underbrace{0, \ldots, 0}_{\sum_{l=i+1}^{n} L_l \text{ times}})^T.$$

Finally, $\boldsymbol{A_1}$ is a weight-matrix of dimension $n \times N$ where row i is defined as

$$(\underbrace{0, \ldots, 0}_{\sum_{l=1}^{i-1} L_l \text{ times}}, a_i(\boldsymbol{w_{i1}}) m_i(\boldsymbol{w_{i1}}), \ldots, a_i(\boldsymbol{w_{iL_i}}) m_i(\boldsymbol{w_{iL_i}}), \underbrace{0, \ldots, 0}_{\sum_{l=i+1}^{n} L_l \text{ times}}).$$

Priors are defined for all regression parameters. We specify $\boldsymbol{\beta} \sim \mathcal{N}(0, \boldsymbol{V_\beta}^{-1})$ with $\boldsymbol{V_\beta} = \zeta \boldsymbol{I}$ and ζ small. Furthermore, denote the global design matrix by $\boldsymbol{C_\rho} = [\boldsymbol{X} : \boldsymbol{B_1(z_1)} : \boldsymbol{B_2(z_2)} : \ldots : \boldsymbol{B_q(z_q)} : \boldsymbol{\Phi(\rho)} : \boldsymbol{E}]$ and the parameter vector $\boldsymbol{\xi} = (\boldsymbol{\beta}^T, \boldsymbol{\theta_1}^T, \ldots, \boldsymbol{\theta_q}^T, \boldsymbol{u}^T, \boldsymbol{\epsilon}^T)^T$. Let $\lambda_{q+1} := \lambda_{spat}$, $\lambda_{q+2} := 1/\sigma^2$ and hence $\boldsymbol{\lambda} = (\lambda_1, \ldots \lambda_q, \lambda_{q+1}, \lambda_{q+2})^T$.

Denote the precision matrix of $\boldsymbol{\xi}$ by $\boldsymbol{Q_\xi^\lambda} = \text{blkdiag}(\boldsymbol{V_\beta}, \lambda_1 \boldsymbol{P_1}, \ldots \lambda_q \boldsymbol{P_q}, \lambda_{q+1} \boldsymbol{\Omega_\rho}, \lambda_{q+2} \boldsymbol{G})$ where $\lambda_{q+2} \boldsymbol{G}$ is the precision matrix of the vector $\boldsymbol{\epsilon}$. Hence, $\boldsymbol{G}$ is a diagonal matrix with diagonal entry i equal to

$$\frac{(\sum_{l=1}^{L_i} a_i(\boldsymbol{w_{il}}) m_i(\boldsymbol{w_{il}}))^2}{\sum_{l=1}^{L_i} (a_i(\boldsymbol{w_{il}}) m_i(\boldsymbol{w_{il}}))^2}.$$

The Bayesian model is given by:

$$
\begin{aligned}
&(y_i|\boldsymbol{\xi}) \sim \text{Poisson}(\mu_i) \text{ with } \boldsymbol{\mu} = \boldsymbol{A_1} \exp(\boldsymbol{C_\rho}\boldsymbol{\xi}),\\
&(\boldsymbol{\xi}|\boldsymbol{\lambda}, \rho) \sim \mathcal{N}(0, (\boldsymbol{Q}_{\boldsymbol{\xi}}^{\boldsymbol{\lambda}})^{-1}),\\
&(\lambda_j|\delta_j) \sim \mathcal{G}\left(\frac{\nu}{2}, \frac{\nu\delta_j}{2}\right) \quad j = 1, \ldots, q+2,\\
&\delta_j \sim \mathcal{G}(a_\delta, b_\delta) \quad j = 1, \ldots, q+2,\\
&p(\rho) \propto \mathcal{G}\left(\frac{\nu}{2}, \frac{\nu\delta_\rho}{2}\right),\\
&\delta_\rho \sim \mathcal{G}(a_\delta, b_\delta),
\end{aligned}
$$

where $\mathcal{G}(a, b)$ is a Gamma distribution with mean a/b and variance a/b^2. This prior specification is selected based on the work of Jullion & Lambert (2007), who proposed hierarchical Gamma priors as a more robust and flexible alternative to traditional Gamma priors. They illustrate that this specification of the hierarchical prior is robust for $a = b$ sufficiently small (e.g. 10^{-5}) and fixed ν (e.g. $\nu = 3$ in this paper).

Note that μ_i in equation (5) is constructed as a summation of exponential terms, deviating from the typical log-link structure commonly used in Poisson regression. However, Johnson et al. (2019) proposed a spatially discrete approximation method that allows for approximating integral (1) in a way that restores the standard log-link structure. This approach will be detailed as well and both methods will be compared in the simulation study presented in Section 3.

2.2.1 A spatially discrete approximation

Similarly as done by Johnson et al. (2019), we can simplify the computation of integral (1) by using a spatially discrete approximation of the log expected incidence $\log(r(\boldsymbol{w}))$, replacing $\log(r(\boldsymbol{w}))$ for every $\boldsymbol{w} \in R_i$ with the weighted average within region R_i. This method is theoretically founded on a first-order Taylor approximation of $r(\boldsymbol{w})$ (see Supplementary

Materials for more details). We can then approximate $\log(r(\boldsymbol{w}))$ in region R_i by:

$$\begin{aligned}\log(r(\boldsymbol{w})) &\approx \int_{R_i} v_i(\boldsymbol{w}) \left(\beta_0 + \sum_{k=1}^{p} \beta_k x_k(\boldsymbol{w}) + \sum_{l=1}^{q} f_l(z_l(\boldsymbol{w})) + s(\boldsymbol{w})\right) d\boldsymbol{w} \\ &= \beta_0 + \sum_{k=1}^{p} \beta_k x^*_{ki} + \sum_{l=1}^{q} f^*_{li} + s^*_i, \end{aligned} \tag{6}$$

with $v_i(\boldsymbol{w}) = m(\boldsymbol{w})/m_i$ and $m_i = \int_{R_i} m(\boldsymbol{w}) d\boldsymbol{w}$, reflecting the potential nonhomogeneous distribution of disease cases within R_i. If the continuous distribution $m(\boldsymbol{w})$ is unavailable, we can alternatively set $v_i(\boldsymbol{w}) = 1/|R_i|$. Further, β_j is the regression coefficient for the aggregate explanatory variable x^*_{ji} $(j = 1, \dots p)$, f^*_{ji} $(j = 1, \dots, q)$ is the aggregated smoothing function and s^*_i the aggregated spatial term.

Combining (1) and (6), the expected counts in region R_i become:

$$\begin{aligned}\mu_i &\approx \int_{R_i} m(\boldsymbol{w}) \exp\left(\beta_0 + \sum_{k=1}^{p} \beta_k x^*_{ki} + \sum_{j=1}^{q} f^*_{ji} + s^*_i\right) d\boldsymbol{w} \\ &= m_i \exp\left(\beta_0 + \sum_{k=1}^{p} \beta_k x^*_{ki} + \sum_{j=1}^{q} f^*_{ji} + s^*_i\right), \end{aligned} \tag{7}$$

which again resembles the log-link structure commonly used in Poisson regression.

To ease notation, we denote by $\widetilde{g(\boldsymbol{w_i})}$ the approximation of the integral $\int_{R_i} v_i(\boldsymbol{w}) g(\boldsymbol{w}) d\boldsymbol{w}$, defined as:

$$\widetilde{g(\boldsymbol{w_i})} = \frac{\sum_{l=1}^{L_i} v_i(\boldsymbol{w_{il}}) a_i(\boldsymbol{w_{il}}) g(\boldsymbol{w_{il}})}{\sum_{l=1}^{L_i} v_i(\boldsymbol{w_{il}}) a_i(\boldsymbol{w_{il}})}.$$

The aggregated spatial term s^*_i can then be written as:

$$s^*_i = \widetilde{s(\boldsymbol{w_i})} = \beta_{w1} \widetilde{w_{1i}} + \beta_{w2} \widetilde{w_{2i}} + \sum_{s=1}^{S} u_s \widetilde{\phi_{is}(\rho)} + \widetilde{\epsilon(\boldsymbol{w_i})}.$$

The terms $(\epsilon^*_1 \dots \epsilon^*_n)^T = \left(\widetilde{\epsilon(\boldsymbol{w_1})}, \dots, \widetilde{\epsilon(\boldsymbol{w_n})}\right)^T$ are again multivariate Gaussian with mean 0 and the variance of ϵ^*_i equal to:

$$\frac{\sum_{l=1}^{L_i} (v_i(\boldsymbol{w_{il}}) a_i(\boldsymbol{w_{il}}))^2 \sigma^2}{(\sum_{l=1}^{L_i} v_i(\boldsymbol{w_{il}}) a_i(\boldsymbol{w_{il}}))^2}.$$

Similarly, the non-linear covariate functions f^*_{ji} can be written as:

$$f^*_{ji} = f_j\widetilde{(z_j(\boldsymbol{w_i}))} = \sum_{k=1}^{K} \theta_{jk} b_{jk}\widetilde{(z_j(\boldsymbol{w_i}))}.$$

and the linear covariate as $x^*_{ki} = \widetilde{x_k(\boldsymbol{w_i})}$.

In matrix notation, the model can be formulated as:

$$\log(\boldsymbol{\mu}) = \boldsymbol{A_2}\left(\boldsymbol{X\beta} + \sum_{j=1}^{q} \boldsymbol{B_j(z_j)\theta}_j + \boldsymbol{\Phi(\rho)u} + \boldsymbol{E\epsilon}^*\right) + \log(m_i), \tag{8}$$

where $\boldsymbol{X}$, $\boldsymbol{E}$, $\boldsymbol{B_j(z_j)}$ and $\boldsymbol{\Phi(\rho)}$ are the continuous design matrices of dimensions $N \times (p+3)$, $N \times n$, $N \times K$ and $N \times S$ respectively, as defined earlier. Row i of weight-matrix $\boldsymbol{A_2}$ of dimension $n \times N$ can now be defined as:

$$(\underbrace{0, \ldots, 0}_{\sum_{l=1}^{i-1} L_l \text{ times}}, \frac{v_i(\boldsymbol{w_{i1}})a_i(\boldsymbol{w_{i1}})}{\sum_{l=1}^{L_i} v_i(\boldsymbol{w_{il}})a_i(\boldsymbol{w_{il}})}, \ldots, \frac{v_i(\boldsymbol{w_{iL_i}})a_i(\boldsymbol{w_{iL_i}})}{\sum_{l=1}^{L_i} v_i(\boldsymbol{w_{il}})a_i(\boldsymbol{w_{il}})}, \underbrace{0, \ldots, 0}_{\sum_{l=i+1}^{n} L_l \text{ times}}).$$

We assume similar priors as before. Denote the global design matrix by $\boldsymbol{C_\rho} = [\boldsymbol{A_2X} : \boldsymbol{A_2B_1} : \boldsymbol{A_2B_2} : \ldots : \boldsymbol{A_2B_q} : \boldsymbol{A_2\Phi(\rho)} : \boldsymbol{A_2E}]$ and the full parameter vector $\boldsymbol{\xi} = (\boldsymbol{\beta}^T, \boldsymbol{\theta_1}^T, \ldots, \boldsymbol{\theta_q}^T, \boldsymbol{u}^T, \boldsymbol{\epsilon}^{*T})^T$. The matrix $\boldsymbol{G}$ is now a diagonal matrix with diagonal entry i equal to

$$\frac{(\sum_{l=1}^{L_i} v_i(\boldsymbol{w_{il}})a_i(\boldsymbol{w_{il}}))^2}{\sum_{l=1}^{L_i} (v_i(\boldsymbol{w_{il}})a_i(\boldsymbol{w_{il}}))^2}.$$

The Bayesian model is then given by:

$$\begin{aligned}
&(y_i|\boldsymbol{\xi}) \sim \text{Poisson}(m_i r_i) \text{ with } \log(\boldsymbol{r}) = \boldsymbol{C_\rho\xi},\\
&(\boldsymbol{\xi}|\boldsymbol{\lambda}, \rho) \sim \mathcal{N}(0, (\boldsymbol{Q^\lambda_\xi})^{-1}),\\
&(\lambda_j|\delta_j) \sim \mathcal{G}\left(\frac{\nu}{2}, \frac{\nu\delta_j}{2}\right) \quad j = 1, \ldots, q+2,\\
&\delta_j \sim \mathcal{G}(a_\delta, b_\delta) \quad j = 1, \ldots, q+2,\\
&p(\rho) \propto \mathcal{G}\left(\frac{\nu}{2}, \frac{\nu\delta_\rho}{2}\right),\\
&\delta_\rho \sim \mathcal{G}(a_\delta, b_\delta).
\end{aligned}$$

2.3 Laplace approximation

For both estimation methods, the posterior of $\boldsymbol{\xi}$ conditional on the penalty vector $\boldsymbol{\lambda}$ and ρ, can be denoted by:

$$\begin{aligned} p(\boldsymbol{\xi}|\boldsymbol{\lambda},\rho;\mathcal{D}) &\propto \mathcal{L}(\boldsymbol{\xi},\rho;\mathcal{D})p(\boldsymbol{\xi}|\boldsymbol{\lambda},\rho) \\ &\propto \exp\left(\sum_{i=1}^{n}(y_i\log(\mu_i)-\exp(\mu_i))\right)\exp\left(-\frac{1}{2}(\boldsymbol{\xi}'\boldsymbol{Q}_{\xi}^{\lambda}\boldsymbol{\xi})\right) \\ &= \exp\left(\sum_{i=1}^{n}(y_i\log(\mu_i)-\exp(\mu_i)-\frac{1}{2}(\boldsymbol{\xi}'\boldsymbol{Q}_{\xi}^{\lambda}\boldsymbol{\xi})\right), \end{aligned}$$

with μ_i equal to (5) and (7) for the exact and approximate method, respectively. The Laplace approximation for the conditional posterior of $\boldsymbol{\xi}$ is $\tilde{p}_G(\boldsymbol{\xi}|\boldsymbol{\lambda},\rho;\mathcal{D}) = \mathcal{N}(\hat{\boldsymbol{\xi}}_\lambda, \hat{\boldsymbol{\Sigma}}_\lambda)$ where $\hat{\boldsymbol{\xi}}_\lambda$ is the posterior mode and $\hat{\boldsymbol{\Sigma}}_\lambda$ corresponds to the inverse of the negative Hessian matrix evaluated at the posterior mode. We can now derive the joint posterior of the hyperparameters $\boldsymbol{\lambda}, \rho$ and $\boldsymbol{\delta}$ similar to Sumalinab et al. (2025). This function is then maximized to obtain an a posteriori estimate for $\boldsymbol{v} = (\log(\lambda_1), \ldots, \log(\lambda_{q+2}))^T$ and $v_\rho = \log(\rho)$. Details can be found in the Supplementary materials.

3 Simulation study

We conducted a simulation study to assess the performance of the proposed estimation method and compared its performance against three existing disaggregation methods, namely the disaggregation approach of Nandi et al. (2023), implemented in the `disaggregation` R-package, ATP Poisson kriging (Payares 2024) and SDALGCP (Johnson et al. 2019). We also compared it with a discrete disease mapping method, namely the BYM model (Besag et al. 1991). For general understanding, we provide a brief overview of these methods, summarizing the key principles.

The method of the `disaggregation` package

Similar to our approach, the method of Nandi et al. (2023) assumes that the observed (aggregated) counts can be considered realizations of a Poisson variable with mean given by equation (1). The underlying intensity $r(\boldsymbol{w})$ for $\boldsymbol{w} \in R_i$ is modeled by:

$$\log(r(\boldsymbol{w})) = \beta_0 + \sum_{k=1}^{p} \beta_k x_k(\boldsymbol{w}) + s(\boldsymbol{w}) + u_i,$$

where u_i is a region-specific i.i.d. Gaussian random effect and $s(\boldsymbol{w})$ a Gaussian random field. The Gaussian random field is modeled using a Matérn covariance function with $\nu = 1$. The approximation of integral (1) then becomes:

$$\mu_i \approx \sum_{l=1}^{N_i} m(\boldsymbol{w_{il}}) \exp\left(\beta_0 + \sum_{k=1}^{p} \beta_k x_k(\boldsymbol{w}) + s(\boldsymbol{w}) + u_i\right),$$

with N_i the number of grid cells for which the centre lies within R_i (i.e. $N_i \leq L_i$). The Gaussian random field is approximated with a Gaussian Markov random field (GMRF) and solved using the stochastic partial differential equation (SPDE) approach (Lindgren et al. 2011), which requires the construction of a mesh.

ATP Poisson kriging

Following Goovaerts (2006), the ATP kriging estimator for the rate $r(\boldsymbol{w})$ with $\boldsymbol{w} \in R_i$ is estimated as a linear combination of the observed rate Y_i/m_i and the rates of $(K-1)$ neighboring units with $K \leq N$:

$$r(\boldsymbol{w}) = \sum_{j=1}^{K} \lambda_i(\boldsymbol{w}) \frac{Y_j}{m_j}.$$

In this equation $\lambda_j(\boldsymbol{w})$ represents the weight assigned to rate Y_j/m_j when estimating the incidence at location $\boldsymbol{w}$. These kriging weights are obtained by solving a system of linear equations, constraining $\sum_{j=1}^{K} \lambda_j(\boldsymbol{w}) = 1$. To solve this system, a model for the point-support spatial covariance function is required. A method for deriving such a model from areal data has been proposed by Goovaerts (2008).

The SDALGCP method

This method proposed by Johnson et al. (2019) again starts from the idea represented by integral (1). However, the intensity $r(\boldsymbol{w})$ is now assumed to follow the model:

$$\log(r(\boldsymbol{w})) = \beta_0 + \sum_{k=1}^{p} \beta_k x_k(\boldsymbol{w}) + s(\boldsymbol{w}),$$

with Gaussian process $s(\boldsymbol{w})$. Using a spatially discrete approximation, the area-level expected counts can be approximated by:

$$\mu_i \approx m_i \exp\left(\beta_0 + \sum_{k=1}^{p} \beta_k x^*_{ki} + s^*_i\right),$$

with x^*_{ki} the aggregated linear covariates and $s^* = (s^*_1, \dots s^*_N)$ a multivariate Gaussian, with an exponential covariance function by default. As this method assumes an underlying Log-Gaussian Cox process instead of a geostatistical model, a suitable number of locations is drawn in every region R_i, according to a class of inhibition processes (Diggle 2013). The aggregated covariates x^*_{ki} and spatial process s^*_i are computed by a weighted average over the sampled points, rather than across all grid cells, as is done by our method and by the Bayesian spatial disaggregation method in the `disaggregation` package. The MCMC method is used to obtain parameter estimates.

The BYM model

Following the BYM model (Besag et al. 1991), the observed counts Y_i are mutually independent Poisson variables, conditional on a Gaussian process S_i, with expected counts modeled by:

$$\mu_i = m_i \exp\left(\beta_0 + \sum_{k=1}^{p} \beta_k x_{ki} + S_i\right),$$

where x_{ki} is the area level covariate and S_i can be written as $S_i = S_{1i} + S_{2i}$. The process S_{1i} is then modeled as:

$$(S_{1i}|S_{1h}, j \neq h) \sim \mathcal{N}\left(n_j^{-1} \sum_{j \sim h} S_{1h}, (\tau_1 n_j)^{-1}\right),$$

where $j \sim h$ denotes that regions R_j and R_h are neighbors and n_j represents the number of neighbors of region R_j. The independent process S_{2i} can be modeled as $S_{2i} \sim \mathcal{N}(0, \tau_2)$.

3.1 Simulation set-up

We simulated the spatial effect over a 100×100 square as a Gaussian random field with variance $\sigma^2 = 0.7$, reflecting a moderate level of spatial variability, and a Matérn covariance function with $\nu = 1$, the default option in the disaggregation method of Nandi et al. (2023). To consider both small and large spatial correlation, the range parameter $(1/\rho)$ was chosen equal to 3 and 10 in scenario (a) and (b) respectively. For both scenarios, we defined the simulation surface as:

$$\log(r(\boldsymbol{w})) = \beta_0 + \beta_1 x_1(\boldsymbol{w}) + s(\boldsymbol{w}),$$

with $\beta_0 = -3,\ \beta_1 = -1.5$, and with spatially structured covariate x_1 simulated to take values approximately within the range $(0, 1.5)$ (see Supplementary Materials Figure S1). Note that we did not include a smooth effect to enable a fair comparison with other disaggregation methods that do not allow for the estimation of flexible non-linear trends.

To explore the ability of the methods to recover the underlying smooth surface, we considered three different configurations where the size of the areas progressively increases: 4×4 (Area 1), 10×10 (Area 2) and 20×20 (Area 3). We then simulated a dataset of area-level counts from a Poisson process with mean given by equation (1).

We performed 100 simulations for every combination of scenario (range equal to 3 or 10) and area configuration. We investigated the performance of our estimation method based on the exact likelihood, which we coin the Spline Spatial Disaggregation Exact Method (henceforth, SSDEM), and the approximation method proposed in Section 2.2.1, called the Spline Spatial Disaggregation Approximation Method (henceforth, SSDAM) using a Matérn covariance function ($\nu = 3/2$). We used 350, 200 and 50 spatial knots $\boldsymbol{\kappa}_S$ for area

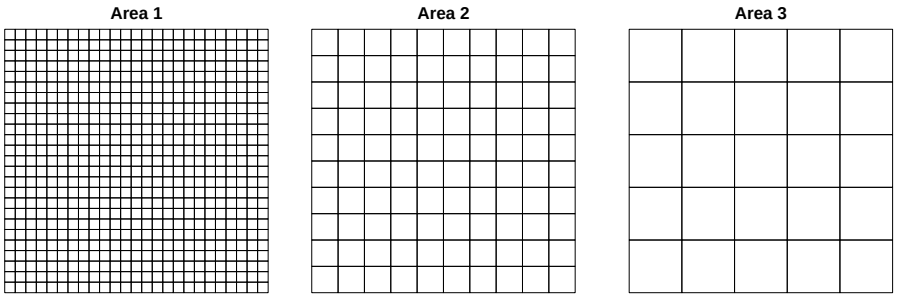

Figure 2: The three different area configurations: Area 1 (625 areas of size 4×4), Area 2 (100 areas of size 10×10) and Area 3 (25 areas of size 20×20).

configuration 1, 2 and 3, respectively. The disaggregation grid resolution is chosen to be 1×1. We evaluated both methods in terms of the RMSE and coverage of the spatial effect and intensity at the grid cell level as well as the average count at the area level. The point estimates are defined as the posterior median, while credible intervals are constructed using the 2.5% and 97.5% percentile of the posterior distribution. More information can be found in the Supplementary Materials. We compared the RMSE and coverage of our methods with results obtained from the `disaggregation` package, the SDALGCP method and ATP Poisson kriging, when available.

3.2 Simulation results

Results for scenario (a) and (b), respectively mild and strong spatial correlation, are given in Table 1. A graphical representation of the RMSEs of the different methods can be found in the Supplementary Materials (Figure S2 and Figure S3). It is important to note that the SDALGCP method failed in 45% of the simulations for scenario (b) with area configuration 1, due to singularity issues. In contrast, none of the other methods encountered errors. Consequently, the results for this specific setting are based on only 55 successful simulations. In the remaining settings, issues were minimal: failure rates were 2% in scenario (b) with area configuration 2 and 3% in scenario (a) with area configuration 1. All other

configurations yielded a 100% success rate across simulations.

The results show that SSDEM and SSDAM perform similarly in terms of RMSE and coverage of the spatial term and continuous incidence, with the latter offering shorter computation times, especially with increasing sample size. As expected, the RMSE at the grid level increases with increasing area size, as less detailed information is available. Figures 3 and 4 show the estimated mean correlation functions in scenarios (a) and (b), respectively. Both the SSDEM and SSDAM methods recover the true correlation function well, particularly in area configurations 1 and 2.

Compared to these, the method of the `disaggregation` package performs similarly in scenario (b) but underperforms in scenario (a), showing higher RMSE and undercoverage of the spatial term for all area configurations. This is also confirmed by Figure 3, showing that the `disaggregation` package overestimates the spatial range for all three area configurations in scenario (a).

The SDALGCP method, using $110,000$ iterations with a burn-in of $10,000$ samples and retaining every 10th sample, yields comparable RMSEs of the grid-level spatial effect in scenario (a), although there is some undercoverage for area configurations 2 and 3. However, the results show increased RMSEs in scenario (b). Figure 4 also shows that the SDALGCP method underestimates the spatial range for area configuration 1 in scenario (b). Finally, as previously noted, the SDALGCP method frequently encountered singularity issues in this specific setting.

The ATP method, producing only disaggregated grid-level counts, yields RMSEs comparable to those of the other methods but exhibits some undercoverage in area configuration 3. Moreover, Figures 3 and 4 show that the correlation function is overestimated in almost all settings. A further examination of the results revealed some extremely high estimated ranges that substantially affected the mean. To address this, the median correlation estimates

are also reported in the Supplementary Materials (Figures S4 and S5). While the median provides values closer to the true correlation function, the ATP method does still not outperform SSDEM or SSDAM in terms of closeness to the true values.

We also compared the estimated spatial variance to the true variance of 0.7 across all settings. As shown in Figure S6 and S7 (Supplementary Materials), all methods perform similarly, though ATP occasionally produces extreme outliers.

At the area level, we can compare the SSDEM, SSDAM and SDALGCP disaggregation methods to the classical BYM method, fitted with INLA. The SSDAM and SDALGCP methods demonstrate RMSE performance comparable to that of the BYM model. For area configuration 3, the SSDEM method exhibits slightly higher RMSEs compared to the BYM method, likely due to the increased computational complexity of the model and the limited number of large areas available. However, for area configurations 1 and 2, its performance is comparable. The ATP and `disaggregation` package, in contrast, do not provide area-level estimates.

Looking at the computation times, the BYM model consistently performs fastest; however, as it is not a disaggregation method, it does not offer any insights into the underlying smooth spatial effect or continuous incidence. Among the disaggregation methods, the `disaggregation` package is the fastest but shows lower performance than our proposed approach when the spatial range is small. Additionally, it does not produce area-level estimates. The ATP method also offers fast computation but lacks the ability to recover the underlying spatial surface and does not support the inclusion of covariates. The SSDAM method remains computationally efficient—typically completing within minutes—and its runtime can be further reduced through parallelization. It performs well across both small and large spatial ranges. The SSDEM method generally exhibits similar performance to SSDAM but requires longer computation times. Finally, the SDALGCP method is the

most computationally intensive, due to MCMC sampling, and underperforms relative to our methods when the spatial range is large. It also does not provide estimates of the continuous incidence.

In the Supplementary Materials, the results of an additional simulation study can be found. In this simulation study, we investigated the quality of the SSDEM and SSDAM method under scenarios with no covariate information and/or lower baseline incidence (by decreasing the intercept β_0). We limited the simulation study to area configuration 2, but we still investigated both small and large spatial range. These results (Table S1) indicate that lowering the baseline incidence increases the RMSE of the spatial surface, which is expected given the reduced response counts. Moreover, the exclusion of covariate information slightly increases the RMSE of the spatial surface as well, but the coverage remains satisfactory. Although the RMSE values of the continuous and discrete incidences are not directly comparable across scenarios, since the underlying incidence levels differ, we can see that the coverage remains generally satisfactory across the considered settings.

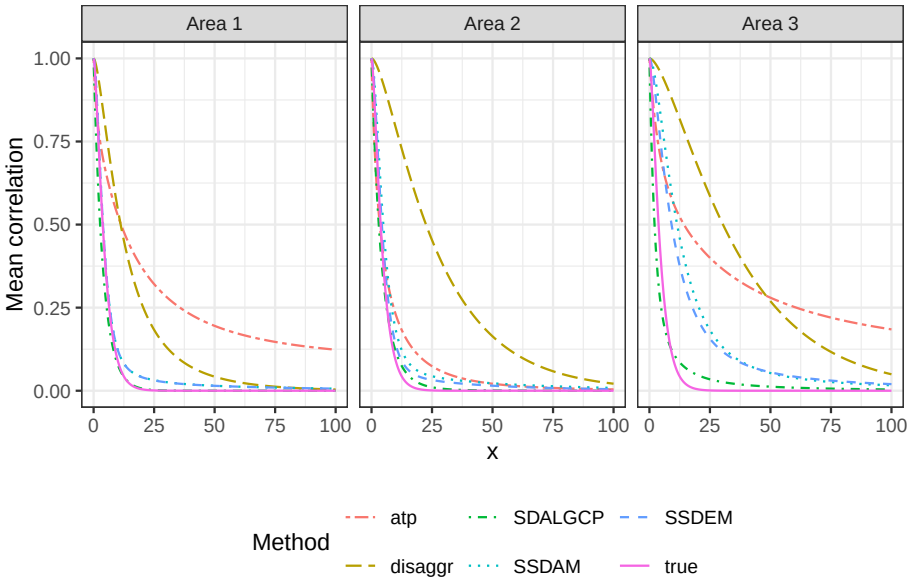

Figure 3: The mean estimated correlation function for a true range of 3 (scenario a) with the different estimation methods, compared with the true correlation function.

Table 1: Simulation results for RMSE and Coverage for the spatial term, continuous incidence (Cont. inc.) and discrete average counts (Discr. inc.) under scenario (a) (range = 3) and (b) (range = 10). The estimation time is given in seconds. Results are given for the 6 different estimation methods (SSDEM, SSDAM, disaggregation, SDALGCP, ATP, BYM).

Scenario	**Area configuration**	**Estimation Method**	**time**	**Spatial term**		**Cont. inc.**		**Discr. inc.**	
				RMSE	Cov	RMSE	Cov	RMSE	Cov
(a) (Range 3)	Area 1 (4×4)	SSDEM	2066	0.71	0.97	0.03	0.96	0.31	0.91
		SSDAM	356	0.71	0.97	0.03	0.95	0.31	0.92
		disaggregation	32	0.76	0.60	0.03	0.84	·	·
		SDALGCP	5513	0.71	0.98	·	·	0.32	0.97
		ATP	132	·	·	0.03	0.87	·	·
		BYM	17	·	·	·	·	0.33	0.94
	Area 2 (10×10)	SSDEM	588	0.75	0.94	0.03	0.93	1.26	0.90
		SSDAM	127	0.75	0.94	0.03	0.93	1.23	0.91
		disaggregation	32	0.80	0.45	0.03	0.65	·	·
		SDALGCP	1481	0.80	0.61	·	·	1.26	0.89
		ATP	143	·	·	0.03	0.88	·	·
		BYM	15	·	·	·	·	1.24	0.94
	Area 3 (20×20)	SSDEM	89	0.80	0.89	0.03	0.87	3.18	0.86
		SSDAM	39	0.80	0.90	0.03	0.88	3.02	0.88
		disaggregation	32	0.82	0.34	0.03	0.41	·	·
		SDALGCP	1203	0.82	0.51	·	·	3.02	0.84
		ATP	246	·	·	0.03	0.69	·	·
		BYM	15	·	·	·	·	2.90	0.94
(b) (Range 10)	Area 1 (4×4)	SSDEM	2111	0.50	0.99	0.02	0.99	0.22	0.90
		SSDAM	385	0.50	0.99	0.02	0.99	0.22	0.92
		disaggregation	32	0.51	0.91	0.02	0.87	·	·
		SDALGCP	5542	0.55	1.00	·	·	0.25	0.99
		ATP	134	·	·	0.02	0.92	·	·
		BYM	17	·	·	·	·	0.24	0.98
	Area 2 (10×10)	SSDEM	605	0.54	0.99	0.02	0.99	1.29	0.90
		SSDAM	131	0.52	0.99	0.02	0.99	1.15	0.93
		disaggregation	32	0.54	0.91	0.02	0.84	·	·
		SDALGCP	1507	0.61	0.87	·	·	1.16	0.94
		ATP	122	·	·	0.02	0.91	·	·
		BYM	15	·	·	·	·	1.24	0.9
	Area 3 (20×20)	SSDEM	104	0.61	0.97	0.02	0.96	3.64	0.89
		SSDAM	42	0.59	0.98	0.02	0.97	3.16	0.91
		disaggregation	31	0.64	0.76	0.02	0.70	·	·
		SDALGCP	1254	0.68	0.80	·	·	3.20	0.91
		ATP	229	·	·	0.02	0.84	·	·
		BYM	14	·	·	·	·	3.18	0.94

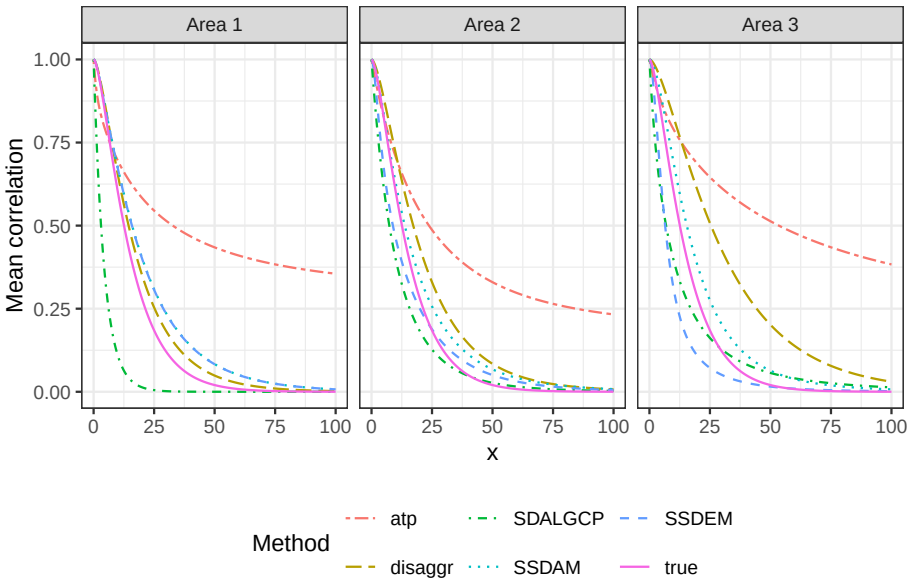

Figure 4: The mean estimated correlation function for a true range of 10 (scenario b) with the different estimation methods, compared with the true correlation function.

4 Data requirements and implementation guidance

Fitting the proposed spatial disaggregation model requires several data components and a number of user-defined choices regarding the number of knots and resolution of the disaggregation grid. This section therefore summarizes the required inputs and outlines practical considerations.

The primary response data consists of area-level counts. Polygon boundaries for these areal units must be available, along with a user-defined grid covering the study region and defining the resolution of the disaggregation process. The choice of this grid resolution is an important modelling decision. A finer grid allows for higher-resolution predictions, but naturally increases computation time, and may exceed the information content, especially when covariates are only available at a lower resolution. Conversely, a lower resolution might oversmooth the spatial variation and undermine the purpose of a disaggregation model. In practice, grid resolution is often driven by the intended use of the predictions,

available precision of the covariates and practical feasibility. As a general guideline, grids substantially finer than the smallest area level are unlikely to be supported, unless fine-scale covariate information at this resolution is available.

Hence, covariate information is preferably available at the desired disaggregation resolution. In practice, covariates that are only available at the area-level can be included as well by assuming constant covariates within each areal unit when mapping to the grid level. However, this approach naturally limits the model's ability to capture small-scale variation driven by covariates. Grid-level offsets are preferred, although not strictly necessary when using the spatially discrete approximation. It is not necessary for every grid cell to contain population i.e. cells with zero population contribute no direct information, but do not invalidate the model. Nevertheless, in practice, it is sensible to avoid excessively fine grids that lead to a large proportion of empty cells, as they offer little inferential benefit.

An important implementation decision is the number and placement of the knots. The number of knots controls the complexity of the spatial effect. Too few knots might result in oversmoothing, while too many knots increase computation time. In practice, the number of knots should not be substantially larger than the number of areas. Simulations showed good performance when using up to 350 knots, with the number of knots set to the minimum of 350 and twice the number of areas, across both weak and strong spatial correlation. Nonetheless, this might also depend on the extent of the geographical region. A sensitivity analysis on this number can be useful for assessing robustness. We conducted a small simulation study to assess the influence of the number of knots, which showed robust results once a sufficiently large number is used (see Supplementary Materials Table S2). To choose the placement of the knots, we first sample a large number of locations in the continuous space, reducing them with a space-filling algorithm (Johnson et al. 1990, Nychka & Saltzman 1998) to the specified number of knots. This way, the procedure is independent of the areal

unit centroids.

5 Data application

We apply our method to two real-life datasets. Firstly, we analyze a dataset on primary biliary cirrhosis (PBC) incidence in Newcastle upon Tyne, UK. The objective of this data application is to compare the obtained disaggregation results using our method with different existing disaggregation methods. Our second data application focuses on mortality rates in Belgium and is motivated by the question of whether meaningful small-area heterogeneity in mortality risk can be recovered from aggregated data. Therefore, while the data are inherently fine-grained, we can aggregate them to a lower resolution, such as the municipality level. Disaggregating these data back to the higher resolution enables us to directly test whether our model successfully reconstructs detailed insights from aggregated data. This application provides a real-world, non-simulated setting to evaluate the disaggregation process. We make use of 350 spatial knots $\boldsymbol{\kappa}_s$ and an exponential covariance function for both data applications.

5.1 Mapping of primary biliary cirrhosis risk

This dataset contains incidence data on PBC at the LSOA level in Newcastle upon Tyne, UK. The dataset is freely available from the `SDALGCP` package in R. It contains PBC rates between 1987 and 1994 as well as the index of multiple deprivation (IMD) for the 545 LSOAs. Since we include our covariates at the grid level, we extracted the IMD value at every grid cell, constructing a spatial raster. These data have previously been analyzed by Johnson et al. (2019). Similar to their model, we included IMD as the only linear covariate. We compared the SSDEM method with the population-weighted SSDAM (SSDAM I) and unweighted SSDAM (SSDAM II) estimation methods as well as with the SDALGCP method

of Johnson et al. (2019), using the population-weighted version, area-to-point Poisson kriging and the estimation method implemented in the `disaggregation` package. To investigate the possible advantage of a non-linear effect, we also fitted the model, using the SSDAM I method, allowing for a smooth effect of IMD (with $df = 10$). Moreover, we compared the area-level estimates with the classical BYM model (Besag et al. 1991). For the SDALGCP method, we used 1100000 iterations of the MCMC algorithm with a burn-in of 100000 samples, retaining every 100th sample, using the code provided by Johnson et al. (2019).

Figure 5a shows a map of the estimated PBC incidence at the LSOA level from all models except `disaggregation` and ATP, which do not produce estimates at the area level. Similarly, an estimated map of the continuous incidence, for all methods except SDALGCP and BYM, can be found in Figure 5b. The Supplementary Materials also contains a figure comparing the estimated spatial surface $\exp(s(x))$ (Figure S8). Furthermore, Figure 6 shows the estimated spatial correlation function from all models assuming an underlying continuous surface (i.e. all models except the BYM model).

It can be seen that the estimated correlation function found by the SSDEM, linear SSDAM I, smooth SSDAM I, SSDAM II and SDALGCP method are highly similar, in contrast to the correlation function found by the `disaggregation` package.

Correlations of the estimated area-level incidence, the estimated spatial effect $\exp(s(x))$ and estimated continuous incidence are also calculated. A high similarity between the SSDEM, SSDAM I (linear and smooth) and SSDAM II methods (correlations above 0.98) is found. There is a relatively high correlation between our methods and the estimates from the SDALGCP model (correlation of approximately 0.87 and 0.70 for the area-level incidence and spatial effect respectively) and the estimates of the `disaggregation` package (correlation of approximately 0.76 and 0.72 for the grid-level incidence and spatial effect respectively). We find a correlation of approximately 0.85 with the BYM model, at the

area-level and a correlation of 0.63 with the ATP model at the continuous incidence level. A detailed overview of the correlations can be found in the Supplementary Materials (Figure S9-S11). To investigate the sensitivity of the chosen covariance structure, we provided a comparison with the Matérn, circular and spherical correlation function, using the (linear) SSDAM I and SSDEM method. This analysis revealed that this choice has minimal impact on the results (Figure S12 and S13 in the Supplementary Materials).

When allowing for a smooth relationship, the effect of IMD is estimated to be increasing but slightly non-linear, although credible intervals are large (see Figure S14 Supplementary Materials). We also provided a comparison of the estimated posterior distributions of the IMD effect for all models assuming a linear effect in the Supplementary Materials (Figure S15).

5.2 Mapping of mortality rates

The dataset provided by Statbel, contains mortality rates from the year 2020, aggregated to the statistical sector level, which is the smallest administrative unit in Belgium, with 19775 sectors. In this analysis, we aggregated these data to obtain a mortality count for each of the 581 municipalities in Belgium. A map of the observed counts at the municipality level as well as the statistical sector level is shown in Figure 8. We downloaded a dataset containing information about the gender and educational attainment in each statistical sector, originating from the Belgian census of 2021 from Belgian Federal Government (2021). We used this dataset to calculate the percentage of males, the percentage of people aged over 15 and the percentage of adults who pursued higher education in each statistical sector. These three variables were included linearly in the model. Missing values were inserted using inverse distance weighting interpolation with the `idw` function in `gstat` in R. Furthermore, we downloaded a dataset containing the average PM_{10} pollution level between 1997 and

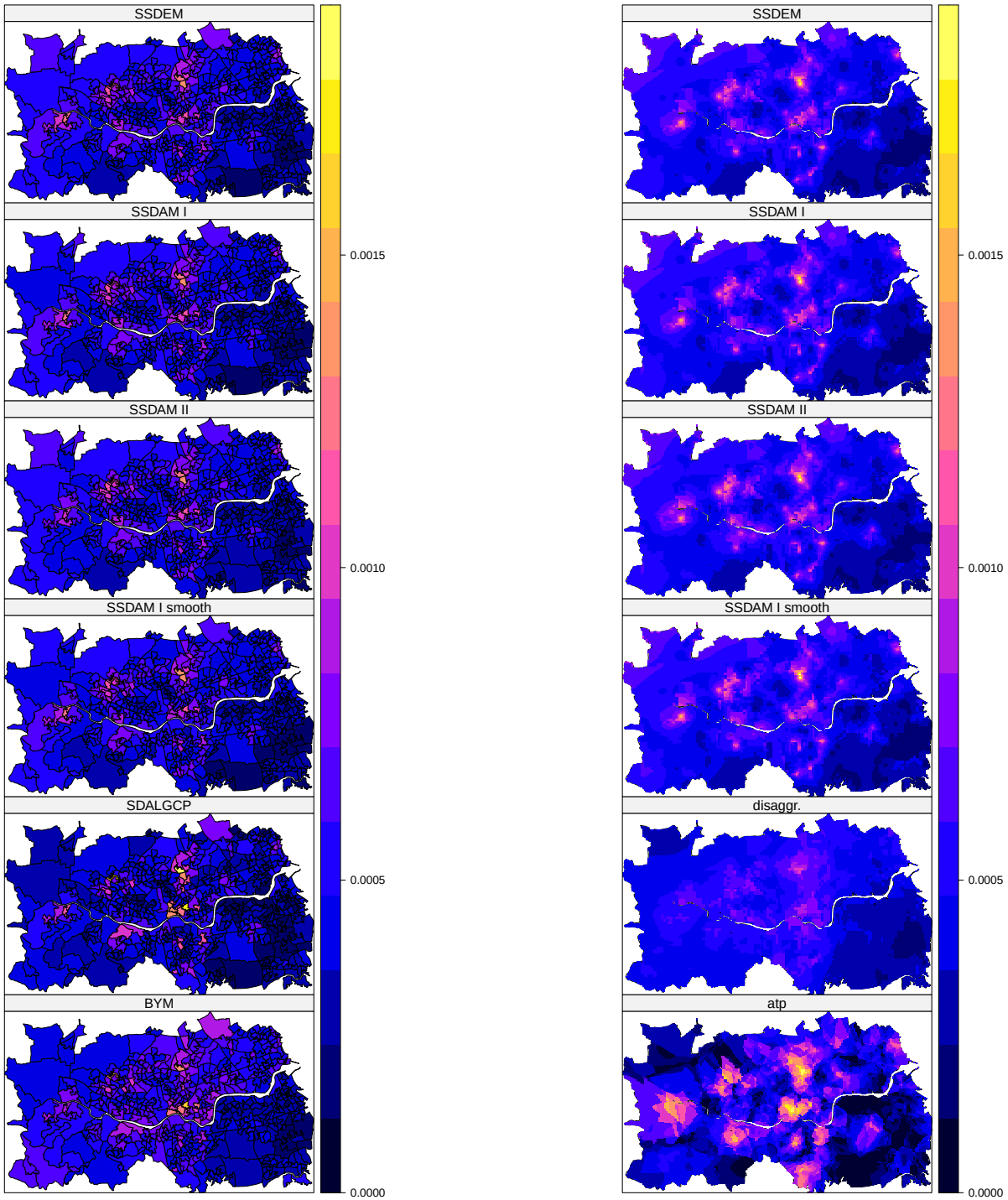

(a) (b)

Figure 5: (a) Maps of the estimated biliary cirrhosis incidence in each LSOA of Newcastle upon Tyne, UK, from: SSDEM, SSDAM I, SSDAM II, SSDAM I smooth, SDALGCP and BYM. (b) Map of the continuous incidence from: SSDEM, SSDAM I, SSDAM II, SSDAM I smooth, disaggregation and ATP.

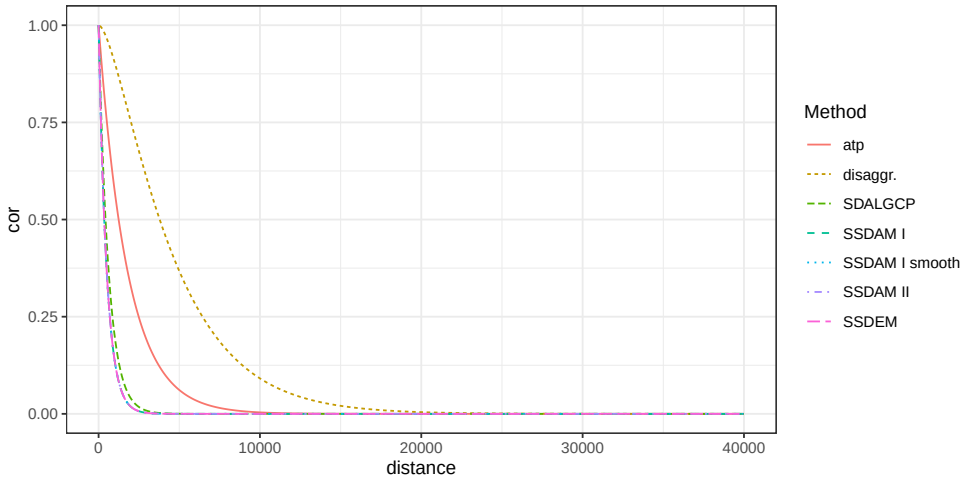

Figure 6: Estimated spatial covariance function from the disaggregation model (red), SDALGCP (brown), SSDAM I (green), SSDAM II (light blue), SSDAM II smooth(dark blue) and SSDEM (pink).

2022 on a 4×4 km grid from Irceline (1997-2022) and a dataset containing the population density on a 1×1 km grid from Statbel (2020). To allow for possible nonlinear effects, we included all covariates as smooth covariates (with 5 df). Since our smallest dimension is a 1×1 km resolution, we opted to create a 1×1 km disaggregation raster and extracted all covariate values at every 1×1 km grid cell (see Figure S16 in the Supplementary Materials). We fitted the model using the population-weighted approximation (SSDAM I).

The results in Figure 7 show that an increase in people aged over 15 leads to a roughly linear increase in expected deaths, while an increase in the percentage of males or percentage of people with higher education results in a roughly linearly decreased expected number of deaths. Besides, the RR for PM_{10} appears to increase non-linearly up to 15 $\mu g/m^3$, with a slight decrease beyond this level. However, given the wide credible intervals, even a linear effect cannot be ruled out.

Furthermore, we calculated the exceedance probability $r(\boldsymbol{w}) > 0.01$ on the 1×1 km grid, where 0.01 represents the average mortality rate at the statistical sector level (Figure S17 Supplementary Materials). However, a key focus of this analysis is determining whether

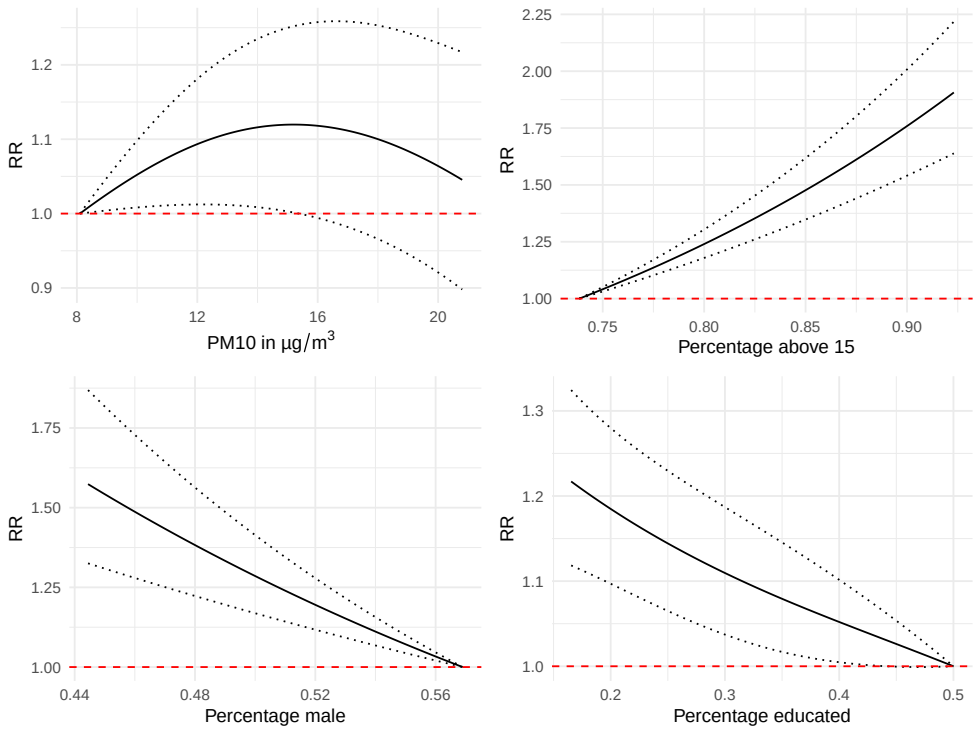

Figure 7: The estimated smooth effect of the four different covariates: PM_{10} (UL), percentage above 15 (UR), percentage of male (LL) and percentage of educated (LR).

incidence can be accurately recovered at the statistical sector level. To achieve this, we estimated the incidence at the 1×1 km raster and aggregated it to the statistical sector level using formula (8), with a modified $\boldsymbol{A_2}$ matrix, connecting the grid cells to the statistical sectors instead of municipalities. We simulated from the posterior predictive distribution and calculated 95% posterior prediction intervals for the number of deaths in every statistical sector. Doing so, a coverage of 96.94% could be retrieved. In the Supplementary materials, Figure S18 shows the estimated number of deaths, together with the 95% prediction intervals and the true number of deaths in 50 randomly selected statistical sectors. A map of the estimated incidence at the statistical sector and municipality level can also be found in Figure 9a and 9b respectively. At the municipality level, the map of the observed mortality (Figure 8) is similar to the map of the estimated incidences. At the statistical sector level, the differences are larger. However, at a fine spatial scale, observed incidences can be highly

variable due to small population sizes and random fluctuations. Therefore, we used INLA to smooth the sector-level incidences, accounting for spatial correlation, in order to reduce the impact of random fluctuations (Figure 9c). Comparing our estimated incidences at the statistical sector level with the INLA-smoothed incidences, a closer fit can be found. We performed a sensitivity analysis by repeating the analysis using (a) a Matérn covariance function and (b) 450 knots instead of 350 knots. Results are robust to these choices. A comparative figure of the estimated fine-scaled incidences can be found in the Supplementary Materials (Figure S19).

We also repeated the analysis using the exact likelihood method (SSDEM) and obtained very similar results. However, the estimation time increased significantly, taking about an hour instead of a few minutes. The results can be found in the Supplementary Materials (Figure S20). Moreover, a comparative figure of the estimated spatial covariance functions is included in the Supplementary Materials as well (Figure S21).

(a) (b)

Figure 8: Observed incidences per 100 000 inhabitants: (a) Statistical sector level, (b) Municipality level.

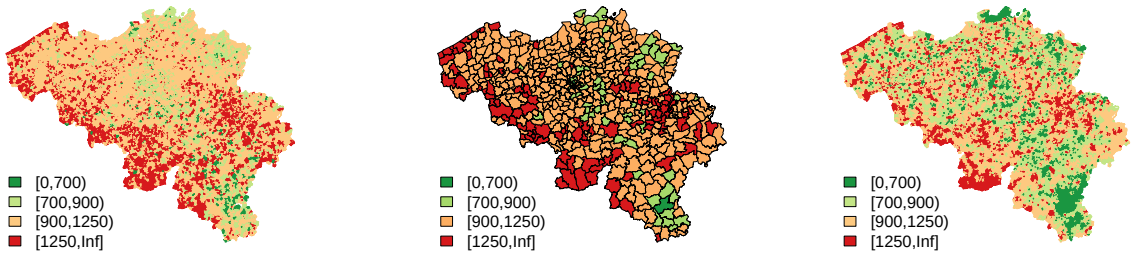

(a) (b) (c)

Figure 9: The estimated incidences per 100 000 inhabitants: (a) Statistical sector level, (b) Municipality level and (c) Smoothed incidences at the statistical sector level (using INLA).

6 Conclusion

In this paper, we introduced a novel spatial disaggregation model, allowing for smooth covariate effects through the use of penalized splines. A spline-based low-rank kriging approximation is used to model the spatial component. Laplace approximations are utilized, offering significant computational advantages over the classical MCMC approach. We compared an estimation method based on the exact likelihood (SSDEM) with a method leveraging a spatially discrete approximation (SSDAM). Simulations showed that both methods perform well. Moreover, leveraging approximations results in significant computational gains, particularly important for large datasets.

Our model can be fitted significantly faster than the SDALGCP model from Johnson et al. (2019), which makes use of the classical MCMC approach. Furthermore, our methods showed slightly better performance in the presence of large spatial correlation. Simulation studies showed that our method outperforms the `disaggregation` method, as the latter tends to overestimate the spatial range in the presence of small spatial correlation. Moreover, our methods avoids mesh constructions, which can be tedious, and it allows the inclusion of smooth covariates. While the `disaggregation` package leverages a template model builder

`TMB` (Kristensen et al. 2016), we derived the analytical calculations underlying the Laplace approximation. We note that our method is slower than the `disaggregation` package, but leveraging SSDAM still allows the model to be fitted within a few minutes. Lastly, in contrast to the PCLM approach of Ayma et al. (2016), we obtained estimates of the underlying spatial correlation structure.

Although we think that our method can be very useful for spatial disaggregation purposes, there are some limitations to the approach. First of all, although it offers the advantage of avoiding mesh-construction, the spline-based low-rank kriging approximation still requires the specification of a number of knots, as well as placement of the knots. Setting the number of knots to the minimum of 350 and twice the number of areas and using a space-filling algorithm, this process is, in our opinion, still more straightforward and less prone to errors compared to mesh-construction. Secondly, the model is relatively complex to estimate and examination of the initial results showed that, especially when using SSDEM, the final estimates of the hyperparameters, and hence also the regression parameters, can be heavily dependent on the initial value of the range parameter. To solve this issue, we decided to run every estimation process multiple times (25 by default), starting from different initial values, and then choose the parameters resulting in the highest posterior likelihood. As shown by the results of the simulation study, this approach works well, both for small and strong spatial correlation. Although this method increases computation time, the simulations show that, especially for SSDAM, the model can still be fitted within a few minutes. Moreover, we can see that, although hyperparameter uncertainty is not taken into account, the coverage of the quantities studied in the simulations, approximately reaches the nominal level. Furthermore, we included a small sensitivity analysis with respect to the priors of the hyperparameters. The results, reported in the Supplementary Materials (Table S3), indicate that posterior inference is stable across different prior specifications.

Finally, we note that the assumption of a continuous latent risk surface defined across the entire study region coincides with standard practice in geostatistical modelling. However, we acknowledge that the interpretation of this risk in uninhabited locations, may not always be practically meaningful, reflecting a conceptual rather than observable quantity.

Despite its limitations, we believe that the introduced model offers a powerful and efficient solution for the increasingly important task of disaggregating count data. Its ability to incorporate penalized smooth covariates, combined with its computational efficiency, makes it a valuable tool not only in epidemiology but also in ecology and environmental science.

Acknowledgements

The computational resources and services were provided by the VSC (Flemish Supercomputer Center), funded by the Research Foundation - Flanders (FWO) and the Flemish Government - department EWI. We acknowledge Statbel for providing the Belgian mortality data.

Funding

TN gratefully acknowledges funding by the Research Foundation - Flanders (grant number G0A3M24N).

Disclosure statement

The authors have declared no competing interest.

Data Availability Statement

The dataset on mortality in Belgium can be requested through Statbel. All other data and code is publicly available on GitHub https://github.com/Rutten-Sara/SpatialDisaggregation.git.

Supplementary materials

Additional theoretical derivations and figures are available in the Supplementary Materials.

References

Ayma, D., Durbán, M., Lee, D. J. & Eilers, P. H. (2016), 'Penalized composite link models for aggregated spatial count data: A mixed model approach', *Spatial Statistics* **17**, 179–198.

Belgian Federal Government (2021), 'Census 2021- population according to: Statistical sector of place of residence, gender and educational attainment', https://data.gov.be/en/datasets/nodeid5535. Accessed: 2025-01-28.

Besag, J., York, J. & Mollié, A. (1991), 'Bayesian image restoration, with two applications in spatial statistics', *Annals of the Institute of Statistical Mathematics* **43**, 1–20.

Brus, D. J., Boogaard, H., Ceccarelli, T., Orton, T. G., Traore, S. & Zhang, M. (2018), 'Geostatistical disaggregation of polygon maps of average crop yields by area-to-point kriging', *European Journal of Agronomy* **97**, 48–59.

Diggle, P. J. (2013), *Statistical Analysis of Spatial and Spatio-Temporal Point Patterns*, CRC Press, New York, NY.

Diggle, P. J., Moraga, P., Rowlingson, B. & Taylor, B. M. (2013), 'Spatial and spatio-

temporal log-gaussian cox processes: Extending the geostatistical paradigm', *Statistical Science* **28**, 542–563.

Eilers, P. H. (2007), 'Ill-posed problems with counts, the composite link model and penalized likelihood', *Statistical Modelling* **7**, 239–254.

Goovaerts, P. (2006), 'Geostatistical analysis of disease data: Accounting for spatial support and population density in the isopleth mapping of cancer mortality risk using area-to-point poisson kriging', *International Journal of Health Geographics* **5**.

Goovaerts, P. (2008), 'Kriging and semivariogram deconvolution in the presence of irregular geographical units', *Mathematical Geosciences* **40**, 101–128.

Gramatica, M., Congdon, P. & Liverani, S. (2021), 'Bayesian modelling for spatially misaligned health areal data: A multiple membership approach', *Journal of the Royal Statistical Society. Series C: Applied Statistics* **70**, 645–666.

Gressani, O. & Lambert, P. (2018), 'Fast Bayesian inference using Laplace approximations in a flexible promotion time cure model based on P-splines', *Computational Statistics & Data Analysis* **124**, 151–167.

Gressani, O., Torneri, A., Hens, N. & Faes, C. (2024), 'Flexible Bayesian estimation of incubation times', *American Journal of Epidemiology* .

Hu, M. & Huang, Y. (2020), 'atakrig: An r package for multivariate area-to-area and area-to-point kriging predictions', *Computers and Geosciences* **139**.

Irceline (1997-2022), 'Pm10 annual mean 1997-2022', http://ftp.irceline.be/rio4x4/. Accessed: 2025-01-28.

Johnson, M., Moore, L. & Ylvisaker, D. (1990), 'Minimax and maximin distance designs.', *Journal of Statistical Planning and Inference* **26**, 131–148.

Johnson, O., Diggle, P. & Giorgi, E. (2019), 'A spatially discrete approximation to log-gaussian cox processes for modelling aggregated disease count data', *Statistics in Medicine* **38**, 4871–4887.

Jullion, A. & Lambert, P. (2007), 'Robust specification of the roughness penalty prior distribution in spatially adaptive Bayesian P-splines models', *Computational Statistics & Data Analysis* **51**(5), 2542–2558.

Kammann, E. E. & Wand, M. P. (2003), 'Geoadditive models', *Journal of the Royal Statistical Society. Series C: Applied Statistics* **52**, 1–18.

Keil, P., Belmaker, J., Wilson, A. M., Unitt, P. & Jetz, W. (2013), 'Downscaling of species distribution models: A hierarchical approach', *Methods in Ecology and Evolution* **4**, 82–94.

Kristensen, K., Nielsen, A., Berg, C. W., Skaug, H. & Bell, B. M. (2016), 'Tmb: Automatic differentiation and laplace approximation', *Journal of Statistical Software* **70**.

Kyriakidis, P. C. (2004), 'A geostatistical framework for area-to-point spatial interpolation', *Geographical Analysis* **36**, 259–289.

Lambert, P. & Gressani, O. (2023), 'Penalty parameter selection and asymmetry corrections to Laplace approximations in Bayesian P-splines models', *Statistical modelling* **23**(5-6), 409–423.

Lang, S. & Brezger, A. (2004), 'Bayesian P-splines', *Journal of Computational and Graphical Statistics* **13**(1), 183–212.

Lee, D. (2023), 'Identifying boundaries in spatially continuous risk surfaces from spatially aggregated disease count data', *Annals of Applied Statistics* **17**, 3153–3172.

Lee, D. J., Durbán, M., Ayma, D. & de Kassteele, J. V. (2022), 'Modeling latent spatio-temporal disease incidence using penalized composite link models', *PLoS ONE* **17**.

Li, Y., Brown, P., Gesink, D. C. & Rue, H. (2012), Log gaussian cox processes and spatially aggregated disease incidence data, *in* 'Statistical Methods in Medical Research', Vol. 21, pp. 479–507.

Lindgren, F., Rue, H. & Lindström, J. (2011), 'An explicit link between gaussian fields and gaussian markov random fields: the stochastic partial differential equation approach'.

Moraga, P., Cramb, S. M., Mengersen, K. L. & Pagano, M. (2017), 'A geostatistical model for combined analysis of point-level and area-level data using inla and spde', *Spatial Statistics* **21**, 27–41.

Nagle, N. N., Sweeney, S. H. & Kyriakidis, P. C. (2011), 'A geostatistical linear regression model for small area data', *Geographical Analysis* **43**, 38–60.

Nandi, A. K., Lucas, T. C., Arambepola, R., Gething, P. & Weiss, D. J. (2023), 'disaggregation: An r package for bayesian spatial disaggregation modeling', *Journal of Statistical Software* **106**.

Nychka, D. & Saltzman, N. (1998), 'Design of air-quality monitoring networks', *Case studies in environmental statistics* pp. 51–76.

Pardo-Igúzquiza, E. & Atkinson, P. M. (2007), 'Modelling the semivariograms and cross-semivariograms required in downscaling cokriging by numerical convolution-deconvolution', *Computers and Geosciences* **33**, 1273–1284.

Payares, D. (2024), 'Ata-poisson-cokriging', https://github.com/DavidPayares/ATA-Poisson-Cokriging. Accessed: April 29, 2025.

Pittiglio, C., Khomenko, S. & Beltran-Alcrudo, D. (2018), 'Wild boar mapping using population-density statistics: From polygons to high resolution raster maps', *PLoS ONE* **13**.

Rue, H., Martino, S. & Chopin, N. (2009), 'Approximate Bayesian inference for latent Gaussian models by using integrated nested Laplace approximations', *Journal of the Royal Statistical Society: Series B (Statistical Methodology)* **71**(2), 319–392.

Statbel (2020), 'Population according to the km² grid (2020)', https://statbel.fgov.be/en/open-data/population-according-km2-grid-2020. Accessed: 2025-01-28.

Sumalinab, B., Gressani, O., Hens, N. & Faes, C. (2025), 'A low-rank bayesian approach for geoadditive modeling', *Spatial Statistics* **68**.

Thompson, R. & Baker, R. J. (1981), Composite link functions in generalized linear models, Technical report.

URL: *https://academic.oup.com/jrsssc/article/30/2/125/6953848*

Truong, P. N., Heuvelink, G. B. & Pebesma, E. (2014), 'Bayesian area-to-point kriging using expert knowledge as informative priors', *International Journal of Applied Earth Observation and Geoinformation* **30**, 128–138.